*Cosmic MASERs: From Protostars to Blackholes*
*IAU Symposium, Vol. 206, 2002*
*V. Migenes and M. J. Reid, eds*

# Full-polarization maps of OH main-line masers in the W51 and G351.78−0.54 star-forming regions

Alice L. Argon, Mark J. Reid

*Harvard-Smithsonian Center for Astrophysics, Cambridge, MA, U.S.A.*

Karl M. Menten

*Max-Planck-Institut für Radioastronomie, Bonn, Germany*

**Abstract.** Full-polarization spectral-line VLBA observations were made of the ground state, main-line, $^2\Pi_{3/2}J = 3/2$ OH masers in two Galactic star-forming regions: the "e1"/"e2" region of W51 and G351.78−0.54. Two especially interesting results are presented. (1) Two of the 27 Zeeman pairs in W51 were found to be associated with unusually strong magnetic fields ($\approx$ 20 mG), more than twice as strong as for any previously reported OH maser. (2) G351.78−0.54 was found to exhibit a high degree of linear polarization (up to 61%), which constrains the three dimensional structure of its magnetic field.

## 1. Observations and Data Reduction

The two Galactic star-forming regions were observed with the Very Long Baseline Array (VLBA) in 1996 March, simultaneously in the two circular polarizations (RCP and LCP) and the two main-line transitions (1665 and 1667 MHz). Both parallel and cross polarizations were correlated so that all four Stokes parameters could be obtained.

We calibrated the data using NRAO's Astronomical Image Processing System (AIPS). The calibration included a standard spectral-line delay calibration (RCP and LCP separately), a determination of the delay offset between RCP and LCP for the reference antenna, a correction for feed leakage, a determination of the absolute orientation of the electric vector using a source with known polarization position angle, and a "phase referencing" of the maser data, whereby the phases of one spectral channel were subtracted from the phases of all other channels. Residual errors (after calibration) are estimated to be $\approx$ 1% and 5° for linear polarization percentages and electric field vector position angles.

## 2. Elliptical Polarization and the Ambient Magnetic Field

An ambient magnetic field (B-field) gives rise to $\pi$ and $\sigma$ transitions. The $\pi$ transitions are linearly polarized and spectrally unshifted while $\sigma$ transitions are elliptically polarized and shifted (split). Since we see no evidence of features

with high degrees of linear polarization but little or no circular polarization, we assume all observed transitions are $\sigma$'s.

The splitting between $\sigma$ components is usually larger than the linewidth and the separation between the RCP and LCP components gives us the B-field strength, e.g., 0.590 km s$^{-1}$ mG$^{-1}$ for the 1665 MHz transition. Also, the frequency shift of RCP with respect to LCP gives us its line-of-sight direction. If RCP appears at a higher frequency than LCP, the B-field's line-of-sight direction is defined as towards the observer.

If a $\sigma$ component is mostly linearly polarized, the B-field is roughly perpendicular to the line-of-sight; if it is mostly circularly polarized, the B-field is roughly parallel to the line-of-sight. In general, the angle between the B-field and the line-of-sight is given by:

$$\theta = cos^{-1}\sqrt{(1-l)/(1+l)},$$

where $l$ is the linear polarization fraction. We note that $\theta$ can also be written as a function of the circular polarization fraction, since our $\sigma$ components are $\approx 100\%$ elliptically polarized. The linear (or circular) polarization fraction locates the magnetic vector on a cone with opening angle $\theta$ with respect to our line-of-sight, but does not give a unique direction. An additional equation:

$$\chi_M = \chi_E \pm 90^\circ,$$

where $\chi_E$ and $\chi_M$ are the position angles of the electric field vector and the B-field's projection onto the plane of the sky, resolves most of the ambiguity. Two possible B-field directions (on opposite sides of the cone) remain.

## 3. W51

Features in W51 were observed to be almost 100% circularly polarized. Twenty-seven Zeeman pairs were identified, and two in the 1665 MHz transition were found to be associated with unusually large magnetic fields, $-21.0$ and $-19.8$ mG. Figure 1 shows spectra of the emission within $\pm 0\farcs012$ of the $(\Delta\theta_x, \Delta\theta_y)$ offsets $(-0\farcs701, 6\farcs170)$ and $(-0\farcs699, 6\farcs200)$ for features 1 and 2, respectively. Offsets are measured with respect to the position: $\alpha = 19^h23^m43\fs930$; $\delta = 14^\circ30'31\farcs46$ (J2000). The features comprising each pair are coincident to within $0\farcs001$, a small fraction of our beam of $0\farcs008$. Aside from some artifacts in the 57$-$60 km s$^{-1}$ LSR velocity range, there is no emission in the vicinity of the two pairs and hence little chance of misidentification. The artifacts are sidelobes of very strong emission in the 57$-$60 km s$^{-1}$ range (Argon, Reid, & Menten 2000); there are no strong features outside this velocity range.

Pulsar and Zeeman-effect observations over six orders of magnitude provide the most reliable means of estimating the B-field strength ($B$) versus total number density ($n$) relationship (Troland & Heiles 1986, Kazès & Crutcher, 1986). These observations suggest that $B \propto \sqrt{n}$. Assuming "interstellar" values of 5 $\mu$G and 1 cm$^{-3}$ for the field strength and number density, respectively, we find that n $\approx$ 2x10$^7$ cm $^{-3}$ for the two pairs. This is on the high end of the allowed densities for OH masers, close to the density at which thermalization is expected to occur (Elitzur, 1992).

https://doi.org/10.1017/S0074180900222729 Published online by Cambridge University Press

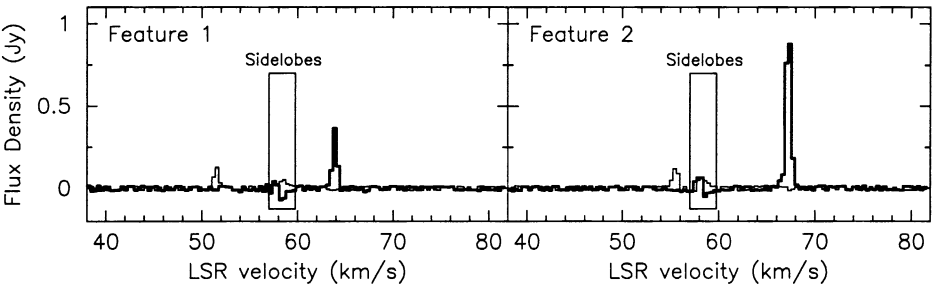


Figure 1. Spectra of the −21.0 mG (left panel) and −19.8 mG (right panel) features in W51. Heavy lines indicate RCP and light lines LCP. Features 1 and 2 are separated by 30 mas (> 3 restoring beams). The minus sign indicates that the line-of-sight direction of the B-field is towards the observer.

## 4. G351.78−0.54

The G351.78−0.54 masers, their measured magnetic fields, and a spherically symmetric model are shown in Figure 2. In the left hand panel Zeeman pairs, represented by "triangles", are shown. The numbers indicate the full strength of the B-field (in mG) and the signs its line-of-sight direction. The dashed line shows a possible dividing line between opposite field directions. In the right hand panel the projections of the B-field vectors onto the plane of the sky (heavy lines) and the angles between the B-field vectors and the line-of-sight (boxed numbers) are shown for the fourteen ≈ 100% elliptically polarized features.

We draw attention to three important patterns in the data: 1) Line-of-sight directions that point towards the observer are spatially separated from those that point away from the observer. 2) B-field vector projections do not follow an obvious global pattern. However, there is a dominant position angle of ≈ 15°, *west* of north. 3) The angles between the B-field vectors and the line-of-sight tend to increase as one moves away from the center of the distribution, which is denoted by the symbol "⊙".

In a simple spherically symmetric model, a "longitudinal bubble", B-field lines enter the "South pole", wrap longitudinally around the bubble's surface, and exit the "North pole". If the South pole is tipped from the plane of the sky by ≈ 30°, there is a small elliptical region in the south where B-field lines point towards the observer and a larger region where they point away from the observer. This agrees with the observations. In addition, if the South pole is rotated eastward by ≈ 15°, the longitudinal B-field lines are roughly parallel to the observed dominant position angle. The model does not, however, predict the correct angles between the B-field vectors and the line-of-sight. The closer one gets to the limb of the bubble, the more the B-field vectors lie in the plane of the sky, the opposite of what this model predicts.

In another spherically symmetric model, a "radial bubble", B-field lines point radially outward. A spatial separation of positive and negative B-field lines, while possible in this model, would require special circumstances. Further, the observed B-field vector projections do not appear radial (and purely radial

https://doi.org/10.1017/S0074180900222729 Published online by Cambridge University Press

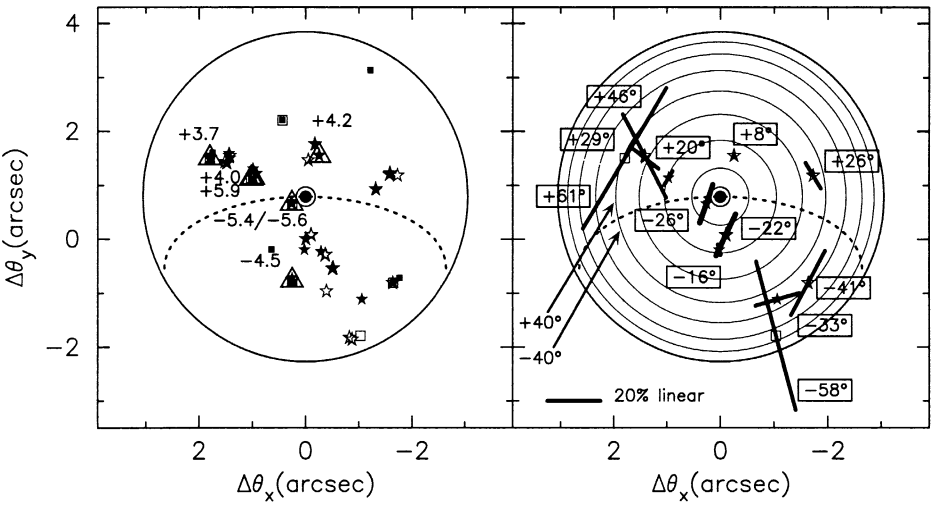


Figure 2. G351.78−0.54 data and spherically symmetric model. Left: Full strength (mG) and line-of-sight directions of B-field (minus is towards observer). Right: Projection of B-field vectors onto plane of sky (lines) and angles between B-field vectors and line-of-sight (boxed numbers). Circular contours refer to the radial bubble model, which is discussed in the text. In both panels "stars" and "squares" represent 1665 and 1667 MHz masers, respectively. Open symbols are RCP and closed symbols LCP. The origin of coordinates is located at $\alpha = 17^h26^m42\overset{s}{.}70$; $\delta = -36°09'17\overset{''}{.}4$ (J2000).

lines would violate Maxwell's equations). The only strength of this model is that the angles between the model's B-field vectors and the line-of-sight (contours separated by 10°) agree with the observed angles (boxed numbers) to within $\approx 12°$, on average. A quasi radial model, e.g., a magnetic dipole, may fit the data reasonably well and will be the subject of future work.

## References

Argon, A. L., Reid, M. J.,& Menten, K. M. 2000, ApJS, 129, 159
Elitzur, M. 1992, Astronomical Masers, Dordrecht: Kluwer Academic
Kazès, I. & Crutcher, R. M. 1986, A&A, 164, 328
Troland, T. H. & Heiles, C. 1986, ApJ, 301, 339

https://doi.org/10.1017/S0074180900222729 Published online by Cambridge University Press